

Control strategies for timestep selection in finite element simulation of incompressible flows and coupled reaction–convection–diffusion processes

A. M. P. Valli¹, G. F. Carey² and A. L. G. A. Coutinho^{3,*},[†]

¹*Computer Science Department, Federal University of Espírito Santo, LCAD, Vitória, ES, Brazil*

²*CFD Laboratory, The University of Texas at Austin, ICES, Austin, TX, U.S.A.*

³*Department of Civil Engineering, Federal University of Rio de Janeiro, COPPE, Rio de Janeiro, Brazil*

SUMMARY

We propose two timestep selection algorithms, based on feedback control theory, for finite element simulation of steady state and transient 2D viscous flow and coupled reaction–convection–diffusion processes. To illustrate performance of the schemes in practice, we solve Rayleigh–Benard–Marangoni flows, flow across a backward-facing step, unsteady flow around a circular cylinder and chemical reaction systems. Numerical experiments confirm that the feedback controllers produce in some cases a very smooth stepsize variation, suggesting that robust control algorithms are possible. These experiments also show that parameter selection can improve timesteps when co-ordinated with the convergence control of non-linear iterations. Further, computational cost of the selection procedures is negligible, since they involve only storing a few extra vectors, computation of norms and evaluation of kinetic energy. Copyright © 2004 John Wiley & Sons, Ltd.

KEY WORDS: timestep selection; control theory; incompressible flows; reaction–convection–diffusion processes

1. INTRODUCTION

With the evolution of numerical methodology to more complex classes of coupled flow and transport problems there has been an increasing need for improved algorithms and other enhancements such as adaptive grid refinement and coarsening. Several adaptive timestep selection strategies have been developed as a means to provide stable accurate transient

*Correspondence to: A. L. G. A. Coutinho, Department of Civil Engineering, COPPE/Federal University of Rio de Janeiro, P.O. Box 68506, Rio de Janeiro, RJ 21945-970, Brazil.

[†]E-mail: alvaro@nacad.ufrj.br

Contract/grant sponsor: CNPq/MCT; contract/grant number: 522692/95-8

Contract/grant sponsor: DoD HPCMP PET; contract/grant number: N62306-01-D-7110

Contract/grant sponsor: Ministry of Education, Brazil

(and steady-state) solutions more efficiently. Analogously, adaptive grid schemes use feedback from the computed solution on a given intermediate grid to ascertain where the grid should be locally refined. We remark that both of these processes (adaptive timestep selection and adaptive grid refinement) can be viewed as examples of feedback control problems. This brings us to the main theme of the present work—the utilization of feedback control algorithms for timestep selection in the simulations of steady state and transient 2D viscous flow and coupled reaction–convection–diffusion processes combined with surface tension effects.

Adaptive techniques for automatic timestep selection are probably the most important means to improve efficiency of a given integration method in the numerical solution of ordinary differential equations. These strategies are usually based on approximate local truncation error measures or on purely heuristic considerations. For example, standard automatic timestep selection algorithms use an estimate of the local truncation error to adjust the stepsize in accordance with a user-specified accuracy requirement, as shown in References [1–4]. Of particular interest here are ODE systems arising from semidiscrete approximation of coupled PDE systems such as those in fluid flow and transport. Gresho *et al.* [5] use a predictor–corrector scheme with a time truncation estimate for integration error control in advection–diffusion problems. Winget and Hughes [6], Johan *et al.* [7] and Jacob and Ebecken [8] develop stepsize selection schemes based on heuristic rules for transient heat conduction, compressible Navier–Stokes equations and structural dynamics problems, respectively. Another strategy for timestep integration is to use control theory. Gustafsson *et al.* [9–11] developed a control approach for adaptive timestep selection and presented an algorithm using the concept of proportional-integral-derivative (PID) control. Both of these studies dealt with traditional ODE systems. A recent review of the field is found in Reference [12].

In this work, we propose two PID timestep control algorithms based on controlling accuracy or the convergence rate of the successive iterations [13–18] for semidiscrete systems arising in PDE applications. The first control utilizes normalized changes in the solution variables of interest (velocities, temperature, concentration, etc.) to compute the local truncation errors. In the second control, the timestep size is limited by the normalized changes in other quantities such as the non-dimensional kinetic energy or by the rate of convergence of the successive approximations. The efficiency of these controls are compared with the heuristic time-stepping strategy developed by Winget and Hughes [6], also implemented in our code. We demonstrate that, with these controllers, we obtain approximate solutions with a smaller number of steps without any significant loss of accuracy. In addition, the controllers also produce in some cases a smooth variation of timesteps, suggesting that a robust control algorithm is possible. These ideas are illustrated for several coupled viscous flow and transport problems. We also provide comparison studies with a digital filter/PID controller presented by Söderlind [19].

The outline of this work is as follows. First, we present the class of transient coupled problems under investigation and briefly the finite element formulations. Then, we discuss the two control algorithms for timestep selection. In Section 4, we present the application problems. In the first problem, we assess the accuracy of the solutions when our controllers are applied to a test problem with known analytical solution. In the second example, we study the performance of the controllers to solve Rayleigh–Benard–Marangoni problems. Then, we solve flow over a backward-facing step and unsteady flow around a circular cylinder with vortex shedding. Finally, we apply the timestep control algorithms to solve non-linear flow and reactive transport as well as chemical reaction systems, we present the main conclusions, and comment on the extension of these ideas to include adaptive meshing.

2. COUPLED VISCOUS FLOW AND TRANSPORT

We consider flow of a viscous incompressible fluid as described by the Navier–Stokes equations coupled to the transport of heat and mass by convection, conduction and reaction in the fluid including surface tension effects. The class of transient coupled problems we are interested in solving may be summarized by the following equations:

$$\frac{\partial \mathbf{u}}{\partial t} + \mathbf{u} \cdot \nabla \mathbf{u} - \nu \Delta \mathbf{u} + \frac{1}{\rho} \nabla p = \mathbf{q} + \mathbf{f}(T, \mathbf{c}) \quad \text{in } \Omega \times I \quad (1)$$

$$\nabla \cdot \mathbf{u} = 0 \quad \text{in } \Omega \times I \quad (2)$$

$$\rho c_p \frac{\partial T}{\partial t} + \rho c_p \mathbf{u} \cdot \nabla T - \nabla \cdot (k \nabla T) = h_1(T, \mathbf{c}) \quad \text{in } \Omega \times I \quad (3)$$

$$\frac{\partial \mathbf{c}}{\partial t} + \mathbf{u} \cdot \nabla \mathbf{c} - \nabla \cdot (\mathbf{K} \nabla \mathbf{c}) = \mathbf{h}_2(T, \mathbf{c}) \quad \text{in } \Omega \times I \quad (4)$$

where Ω is the flow domain, $I = [0, \bar{t}]$ the time interval, \mathbf{u} the velocity vector, p the pressure, $\nu = \mu/\rho$ the kinematic viscosity, ρ the density, \mathbf{q} is an applied body force, $\mathbf{f}(T, \mathbf{c})$ is a temperature (T) and species concentration (\mathbf{c}) dependent body force, c_p the specific heat, k the thermal conductivity, $h_1(T, \mathbf{c})$ and $\mathbf{h}_2(T, \mathbf{c})$ are non-linear reaction source/sink terms and \mathbf{K} is the diffusion tensor. The initial conditions of the problem are $\mathbf{u}(0) = \mathbf{u}_0$, $T(0) = T_0$, $\mathbf{c}(0) = \mathbf{c}_0$, and we consider the following boundary conditions:

- velocities or free surface boundary conditions

$$\mathbf{u} = \mathbf{u}_w \quad \text{or} \quad \nu \nabla \mathbf{u} \cdot \mathbf{n} = 0 \quad \text{on } \partial\Omega_1 \quad (5)$$

$$\nu \nabla \mathbf{u} \cdot \mathbf{n} = \mathbf{\Gamma}(T, \mathbf{c}) \quad \text{on } \partial\Omega_2 \quad (6)$$

- temperature, flux or mixed boundary conditions

$$T = T_w \quad \text{or} \quad k \nabla T \cdot \mathbf{n} = 0 \quad \text{on } \partial\Omega_3 \quad (7)$$

$$k \nabla T \cdot \mathbf{n} = h_c(T - T_e) \quad \text{on } \partial\Omega_4 \quad (8)$$

- species concentration, flux and mixed boundary conditions

$$\mathbf{c} = \mathbf{c}_w \quad \text{or} \quad \mathbf{K} \nabla \mathbf{c} \cdot \mathbf{n} = \mathbf{0} \quad \text{on } \partial\Omega_5 \quad (9)$$

$$-\mathbf{K} \nabla \mathbf{c} \cdot \mathbf{n} = \gamma \mathbf{c} - \mathbf{\Psi} \quad \text{on } \partial\Omega_6 \quad (10)$$

where \mathbf{n} is a unit normal vector, and we suppose that the boundary $\partial\Omega$ of the domain may be divided into $\partial\Omega_1$ to $\partial\Omega_6$, on which conditions can be imposed. Functions \mathbf{u}_w , $\mathbf{\Gamma}$, $\mathbf{\Psi}$ are specified and h_c , γ are known parameters.

Let us first consider the spatial discretization of the viscous flow equation. Introducing a finite element discretization and basis on a uniform discretization Ω_h of quadrilateral elements, the semidiscrete projection of the penalized variational formulation of the Navier–Stokes equations (1) and (2) reduces to: for $0 < \varepsilon \ll 1$, find $\mathbf{u}_h^\varepsilon \in V^h$ satisfying the initial condition with $\mathbf{u}_h^\varepsilon = \mathbf{u}_w$ on $\partial\Omega_{1h}$ such that [20, 21]

$$\begin{aligned} & \int_{\Omega_h} \left(\frac{\partial \mathbf{u}_h^\varepsilon}{\partial t} \cdot \mathbf{v}_h + \nu \nabla \mathbf{u}_h^\varepsilon : \nabla \mathbf{v}_h + (\mathbf{u}_h^\varepsilon \cdot \nabla) \mathbf{u}_h^\varepsilon \cdot \mathbf{v}_h \right) d\Omega + \frac{1}{\varepsilon} \mathbf{I}(\nabla \cdot \mathbf{u}_h^\varepsilon)(\nabla \cdot \mathbf{v}_h) \\ & = \int_{\Omega_h} (\mathbf{q} + \mathbf{f}(T_h, \mathbf{c}_h)) \cdot \mathbf{v}_h d\Omega + \int_{\partial\Omega_{2h}} \Gamma - (T_h, \mathbf{c}_h) \cdot \mathbf{v}_h dl \end{aligned} \quad (11)$$

for all $\mathbf{v}_h \in V^h$ with $\mathbf{v}_h = \mathbf{0}$ on $\partial\Omega_{1h}$, where \mathbf{I} denotes reduced numerical integration, ε is the penalty parameter, $\partial\Omega_h$ is the finite element approximation of the boundary, and $\partial\Omega_{h1}$ to $\partial\Omega_{h6}$ approximate $\partial\Omega_1$ to $\partial\Omega_6$, respectively. This leads to the following non-linear semidiscrete system of ordinary differential equations:

$$\mathcal{M} \frac{d\mathbf{U}}{dt} + \nu \mathcal{A} \mathbf{U} + \hat{\mathcal{N}}(\mathbf{U}) + \frac{1}{\varepsilon} \mathcal{B} \mathbf{U} = \mathcal{F}(\mathbf{T}, \mathbf{C}) \quad (12)$$

where matrices \mathcal{M} , \mathcal{A} , $\hat{\mathcal{N}}$, \mathcal{B} correspond to the respective mass, viscous, inertial and penalty terms on the left in (11) and \mathcal{F} corresponds to the source term on the right. The semidiscrete systems for the heat and mass transfer equations are constructed similarly. For example, the finite element formulation for the mass transfer equation of a representative single species c_s , $s = 1, 2, \dots, n_s$ of (4) is

$$\begin{aligned} & \int_{\Omega_h} \left(w_h \left(\frac{\partial c_{hs}}{\partial t} + u_{hi} \frac{\partial c_{hs}}{\partial x_i} \right) + \frac{\partial w_h}{\partial x_i} k_{ij}^s \frac{\partial c_{hs}}{\partial x_j} - w_h h_{2s}(T_h, \mathbf{c}_h) \right) d\Omega \\ & + \sum_{e=1}^E \int_{\Omega_e} \tau \frac{u_{hm}}{\|\mathbf{u}_h\|} \frac{\partial w_h}{\partial x_m} \left(\frac{\partial c_{hs}}{\partial t} + u_{hi} \frac{\partial c_{hs}}{\partial x_i} - \frac{\partial}{\partial x_i} \left(k_{ij}^s \frac{\partial c_{hs}}{\partial x_j} \right) - h_{2s}(T_h, \mathbf{c}_h) \right) d\Omega \\ & = \int_{\partial\Omega_{6h}} w_h (\gamma c_{hs} - \Psi_s) dl \quad \text{for all } w_h \in W^h \end{aligned} \quad (13)$$

where W^h is the finite element test space for the transport problem, the first integral represents the Galerkin formulation of the problem and the second integral is the SUPG stabilization term added to the variational formulation [22]. The last integral in (13) enforces the mixed boundary condition (10) and k_{ij}^s , $i, j = 1, 2$, is the diffusion tensor for species component s . The resulting semi-discrete ODE system for the nodal concentration vector \mathbf{C} has the form

$$\hat{\mathcal{M}} \frac{d\mathbf{C}}{dt} + \mathcal{R}(\mathbf{U})\mathbf{C} + \mathcal{E}\mathbf{C} = \mathcal{H}(\mathbf{C}) \quad (14)$$

where matrices $\hat{\mathcal{M}}$, \mathcal{R} and \mathcal{E} correspond to the respective mass, convective and diffusive terms on the left in (13) and \mathcal{H} corresponds to the source term on the right. A similar

semidiscrete SUPG system follows from (3) for temperature. This yields a coupled set of semidiscrete systems for nodal velocity, species concentration and temperature. The resulting coupled semidiscrete systems are integrated using a standard θ -method $0 \leq \theta \leq 1$, where $\theta = 0$ corresponds to the forward Euler scheme, $\theta = \frac{1}{2}$ the trapezoidal Crank–Nicolson type scheme and $\theta = 1$ the backward Euler scheme. In the numerical studies presented later, the second-order implicit scheme ($\theta = \frac{1}{2}$) is used. Timestep selection is based on the PID control described later.

Within each timestep we must solve a coupled non-linear algebraic system associated with the discretized flow and transport equations. The main coupling between the flow and transport subsystems enters weakly through the dependence of the source term in the flow equations on the temperature and concentration and the convective velocity in the species/temperature transport. Since the class of applications here does not involve high speed flow a corresponding iterative block decoupling of the subsystems within each timestep will be effective. That is, we can decouple the respective discretized flow and transport systems by a successive approximation scheme in which the source term is ‘lagged’ in the flow equation and the computed velocity iterate is then used in the discretized transport subsystems. This successive approximation iteration is then repeated until convergence.

The respective flow and transport subproblems (resulting from the successive approximation decoupling) are non-linear. In the present scheme the non-linearity from the inertial term in the flow equation subsystem (12) is weak so we use an iterative successive approximation to linearize $\hat{\mathcal{N}}$ in (12) as

$$\hat{\mathcal{N}}(\mathbf{U}) \approx \mathcal{D}(\mathbf{U}_{k-1})\mathbf{U}_k = \int_{\Omega_h} (\mathbf{u}_{h,k-1}^e \cdot \nabla) \mathbf{u}_{h,k}^e \cdot \mathbf{v}_h \, d\Omega \quad (15)$$

with initial iterates given by the solution at the previous step. For each successive approximation $k = 1, 2, \dots$ within timestep we have to solve linear systems of the form

$$\mathcal{P}\mathbf{U}_k^n = \mathcal{Q} \quad (16)$$

with

$$\mathcal{P} = \mathcal{M} + \frac{\Delta t}{2} \left(v\mathcal{A} + \mathcal{D} + \frac{1}{\varepsilon}\mathcal{B} \right) \quad (17)$$

$$\mathcal{Q} = \left(\mathcal{M} - \frac{\Delta t}{2} \left(v\mathcal{A} + \mathcal{D} + \frac{1}{\varepsilon}\mathcal{B} \right) \right) \mathbf{U}_k^{n-1} + \frac{\Delta t}{2} (\mathcal{F}^n + \mathcal{F}^{n-1}) \quad (18)$$

where n denotes the time index, and $\mathcal{F}^n = \mathbf{q}^n + \mathbf{f}$ where \mathbf{f} is evaluated at the current iterate of \mathbf{T} and \mathbf{C} . Solutions of the resulting linear systems are obtained using a direct frontal solver [23].

The velocity solution is then used as the convective coefficient in the subsequent transport systems such as (14). Since the reaction term \mathcal{H} in (14) is a non-linear function of the unknown species solution, we have to solve a non-linear system of the form

$$\mathcal{L}(\mathbf{C}^n) = 0 \quad (19)$$

where

$$\mathcal{L}(\mathbf{C}^n) = \left(\hat{\mathcal{M}} + \frac{\Delta t}{2} (\mathcal{R}(\mathbf{U}^n) + \mathcal{E}) \right) \mathbf{C}^n - \frac{\Delta t}{2} \mathcal{H}^n + \mathcal{I} \quad (20)$$

with

$$\mathcal{I} = - \left(\hat{\mathcal{M}} - \frac{\Delta t}{2} (\mathcal{R}(\mathbf{U}^{n-1}) + \mathcal{E}) \right) \mathbf{C}^{n-1} - \frac{\Delta t}{2} \mathcal{H}^{n-1} \quad (21)$$

and n denotes the timestep index. The non-linear system (19) is solved by Newton's method in the present study. The starting iterate is the solution from the most recent subsystem solve. Given \mathbf{C}_0^n , \mathbf{U}^{n-1} and \mathbf{U}^n , for $k = 1, 2, \dots$, solve linear systems of the form

$$\mathcal{J}(\mathbf{C}_k^n - \mathbf{C}_{k-1}^n) = -\mathcal{V} \quad (22)$$

with

$$\mathcal{J} = \left(\hat{\mathcal{M}} + \frac{\Delta t}{2} (\mathcal{R}(\mathbf{U}^n) + \mathcal{E}) \right) - \frac{\Delta t}{2} \frac{\partial \mathcal{H}_{k-1}^n}{\partial \mathbf{C}^n} \quad (23)$$

and

$$\mathcal{V} = \left(\hat{\mathcal{M}} + \frac{\Delta t}{2} (\mathcal{R}(\mathbf{U}^n) + \mathcal{E}) \right) \mathbf{C}_{k-1}^n - \frac{\Delta t}{2} \mathcal{H}_{k-1}^n + \mathcal{I} \quad (24)$$

where \mathcal{I} is defined in (21) and $\mathcal{H}_{k-1}^n = \mathcal{H}(\mathbf{T}_{k-1}^n, \mathbf{C}_{k-1}^n)$. Here the solution of the linear systems (22) are also obtained using a direct frontal solver [23]. A similar approach is applied to the thermal subsystem and the solutions used to update the source term in the flow equation.

In the preceding discussion we have outlined an algorithm for decoupled solution of the subsystems within each timestep. Such a decoupled scheme is appropriate when the PDE subsystems are weakly coupled, as in the cases described in later numerical experiments. For situations where the coupling is strong it may be preferable to solve the problem within each timestep as a fully coupled system or use other algorithms. The situation is then quite complex because the cost of the fully coupled non-linear algebraic solution is much more expensive. It is clearly also possible to construct other variants of the scheme described here. For example, one can consider approximate solution of the decoupled problem with a single pass where the coupling source term is treated explicitly using the value from the previous timestep. Such an approach is appealing when the timescales of the subsystems differ significantly or if other non-linearities in the systems are comparatively more significant than the coupling non-linearity. The non-linearity can restrict the timestep by rejecting and halving timesteps where non-linear convergence is not attained in a subsystem solve. If the problem is due to disparate timescales then subcycling is effective with different size timesteps on different subsystems [24]. It is clear from these remarks that the choice of a best algorithm is inherently problem dependent. In the numerical studies we consider both multisweep and single sweep decoupling within a timestep and comment on their behaviour.

Clearly, other integrators are possible and may be advisable in some situations, but similar PID timestep control strategies to those considered here can again be applied. In the next section we discuss the form of timestep control utilized in the present scheme and numerical studies.

3. CONTROL STRATEGIES

Most timestep schemes are based on controlling accuracy as determined by truncation error estimates (e.g. Prediction–Modification–Correction). The objective of timestep selection is to minimize the computational effort to construct an approximate solution of a given problem in accordance with a desired accuracy. Gustafsson *et al.* [9–11] showed that stepsize selection can be viewed as an automatic control problem with a PID controller defined as

$$\Delta t_{n+1} = \left(\frac{e_{n-1}}{e_n} \right)^{k_p} \left(\frac{\text{tol}}{e_n} \right)^{k_i} \left(\frac{e_{n-1}^2}{e_n e_{n-2}} \right)^{k_D} \Delta t_n \quad (25)$$

where tol is some input tolerance, e_n is the measure of the change of the quantities of interest in time t_n , and k_p , k_i and k_D are the PID parameters. Figure 1 shows a block diagram of the feedback control problem. An estimate of the solution change is compared with the specified accuracy requirement, and the result is fed back to calculate the new time step. The controller tries to select the stepsize such that e_n comes as close as possible to the input tolerance, tol , along a smooth curve.

Gustafsson and Söderlind [25] establish a model for controlling the convergence rate of the iterative method that relates the convergence rate to the stepsize. Assuming that the stepsize is limited by the convergence rate of non-linear iterations, the new stepsize should be chosen as

$$\Delta t_{n+1} = \frac{\alpha_{\text{ref}}}{\alpha} \Delta t_n \quad (26)$$

where α_{ref} is a reference rate of convergence and α is an estimated rate of convergence. Now the controller tries to keep the estimated convergence rate as close as possible to a reference value, α_{ref} . In general, any value $0.2 < \alpha_{\text{ref}} < 0.4$ would be acceptable, and $\alpha_{\text{ref}} \approx 0.2$ gives performance near to optimal [25]. The estimated rate of convergence is calculated using three consecutive iterates for the velocities, \mathbf{u}_{n-2} , \mathbf{u}_{n-1} , and \mathbf{u}_n , as follows:

$$\alpha = \max_n \alpha_n = \max_n \frac{\|\mathbf{u}_n - \mathbf{u}_{n-1}\|}{\|\mathbf{u}_{n-1} - \mathbf{u}_{n-2}\|} \quad (27)$$

It is necessary to co-ordinate the convergence control algorithm (26) with the stepsize control strategy (25) so that efficiency is maintained. We propose two timestep control algorithms.

The first control uses the changes in velocities, temperature and concentrations, and can be motivated based on the need to control accuracy with respect to time in the specific solution

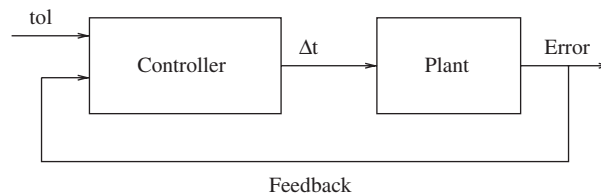


Figure 1. Stepsize selection viewed as a control problem.

variables. The *Control 1* is defined by

$$\Delta t = \left(\frac{e_{n-1}}{e_n} \right)^{k_p} \left(\frac{1}{e_n} \right)^{k_i} \left(\frac{e_{n-1}^2}{e_n e_{n-2}} \right)^{k_D} \Delta t_{\text{prev}} \quad (28)$$

with

$$e_n = \max(e_u, e_T, e_c) \quad (29)$$

where

$$e_u = \frac{e_u^*}{\text{tol}_u}, \quad e_u^* = \frac{\|\mathbf{U}^n - \mathbf{U}^{n-1}\|}{\|\mathbf{U}^n\|} \quad (30)$$

$$e_T = \frac{e_T^*}{\text{tol}_T}, \quad e_T^* = \frac{\|\mathbf{T}^n - \mathbf{T}^{n-1}\|}{\|\mathbf{T}^n\|} \quad (31)$$

$$e_c = \frac{e_c^*}{\text{tol}_c}, \quad e_c^* = \frac{\|\mathbf{C}^n - \mathbf{C}^{n-1}\|}{\|\mathbf{C}^n\|} \quad (32)$$

and Δt represents the new timestep size, Δt_{prev} is the timestep size at the previous step, and tol_u , tol_T and tol_c are user supplied tolerances corresponding to the normalized changes in velocities, temperature and concentration vectors, respectively. The control formula (28) may be written in the equivalent form [19]

$$\Delta t = \left(\frac{1}{e_n} \right)^{k_i + k_p + k_D} \left(\frac{1}{e_{n-1}} \right)^{-(k_p + 2k_D)} \left(\frac{1}{e_{n-2}} \right)^{k_D} \Delta t_{\text{prev}} \quad (33)$$

which is expressed in terms of present and past control errors only. Depending on the way the norm that measures the error is implemented, this formula is preferable. However, we observe in our numerical experiments that the results with this alternative formula are essentially identical. Thus, we use the control formula given by (28).

In the second control, the size of the timestep is limited by the changes in the kinetic energy or by the rate of convergence of the successive approximations. The *Control 2* is given by

$$\Delta t = \min(\Delta t_\alpha, \Delta t_r) \quad (34)$$

where

$$\Delta t_\alpha = \frac{\alpha_{\text{ref}}}{\alpha} \Delta t_{\text{prev}} \quad (35)$$

$$\Delta t_r = \left(\frac{e_{n-1}}{e_n} \right)^{k_p} \left(\frac{1}{e_n} \right)^{k_i} \left(\frac{e_{n-1}^2}{e_n e_{n-2}} \right)^{k_D} \Delta t_{\text{prev}} \quad (36)$$

```

1. Input data:  $U^{n-1}$ ,  $U^n$ ,  $T^{n-1}$ ,  $T^n$ ,  $C^{n-1}$ ,  $C^n$ ,  $K^{n-1}$ ,  $K^n$ ,  $t$ ,  $\Delta t$ ,  $n$ ,  $\alpha$ ,  $nsa$ .
2. Control data:  $\Delta t_{min}$ ,  $\Delta t_{max}$ ,  $k_P$ ,  $k_I$ ,  $k_D$ ,  $tol_u$ ,  $tol_T$ ,  $tol_c$ ,  $tol_K$ ,  $nsa_{max}$ ,
    $\alpha_{ref}$ ,  $control$ .
3. Initialize variables:  $e_{n-2} \leftarrow 1.0$ ,  $e_{n-1} \leftarrow 1.0$ ,  $\Delta t_{prev} \leftarrow \Delta t_{min}$ ,  $nrej \leftarrow 0$ .
4. If  $control = 1$  then
   compute  $e_n$  using (29)-(32)
   else
   compute  $e_n$  using (37).
5. If  $((e_n > 1.0)$  or  $(nsa > nsa_{max}))$  and  $(\Delta t > \Delta t_{min})$  then
   reject the timestep:
   (a)  $nrej \leftarrow nrej + 1$ 
   (b)  $U^n \leftarrow U^{n-1}$ ,  $T^n \leftarrow T^{n-1}$ ,  $C^n \leftarrow C^{n-1}$ ,  $K^n \leftarrow K^{n-1}$ 
   (c)  $t \leftarrow t - \Delta t$ 
   (d)  $n \leftarrow n - 1$ 
   (e)  $factor = \frac{1}{e_n}$ 
   (f) if  $(factor > 0.8)$   $factor = 0.8$ 
   (g)  $\Delta t \leftarrow \max(factor \Delta t, \Delta t_{min})$ 
   (h)  $\Delta t_{prev} \leftarrow \Delta t^2 / \Delta t_{prev}$ 
else
(i) compute  $\Delta t \leftarrow (\frac{e_{n-1}}{e_n})^{k_P} (\frac{1}{e_n})^{k_I} (\frac{e_{n-1}^2}{e_n e_{n-2}})^{k_D} \Delta t_{prev}$ 
(j) If  $control = 2$  then
   (j1) compute  $\Delta t_\alpha$  using (35)
   (j2)  $\Delta t \leftarrow \min(\Delta t_\alpha, \Delta t)$ 
(k)  $\Delta t \leftarrow \max(\Delta t, \Delta t_{min})$ 
(l)  $\Delta t \leftarrow \min(\Delta t, \Delta t_{max})$ 
(m)  $\Delta t_{prev} \leftarrow \Delta t$ 
(n)  $e_{n-2} \leftarrow e_{n-1}$ ,  $e_{n-1} \leftarrow e_n$ 
endif

```

Figure 2. Algorithm for Control 1 and 2.

and

$$e_n = \frac{e_K^*}{tol_K}, \quad e_K^* = \frac{\|K^n - K^{n-1}\|}{\|K^n\|}, \quad K = \int_{\Omega} \frac{(u^{*2} + v^{*2})}{2} d\Omega \quad (37)$$

Here, tol_K is a given tolerance corresponding to the normalized changes in kinetic energy, and u^* and v^* are the non-dimensional velocity components. The motivation in choosing this control for the kinetic energy is related to an interest in the qualitative behaviour of the solution as different cell structures, steady-state solutions, periodic solutions or aperiodic solutions arise.

Our control algorithms may be summarized by the steps in Figure 2. The algorithm for controlling the timestep has two main parts. First, a step size is assumed, and using the newly

computed solution, an *a posteriori* estimate is made of the error in the step. Second, this error measure is used to accept or reject the solution and modify the timestep accordingly. If the error is unacceptable, the new solution is discarded and we restart the time integration in the previous step with a scaled timestep size based on the magnitude of the error relative to the tolerance. In our algorithm, if the sequence of iterates of the non-linear system is converging at a slow rate, the timestep is also rejected. That is, if the number of successive approximations n_{sa} is greater than the maximum number of successive approximations allowed $n_{sa_{max}}$, the step size is rejected. If the error is acceptable, a new timestep is calculated using (28) or (34) and we proceed with the time integration.

To prevent an excessive growth or reduction of the step size Δt , we supply timestep limiters Δt_{min} and Δt_{max} which limit the control signal (anti-windup effect [26]). The effect of the anti-windup is to reduce both overshoot and the control effort in the feedback system. In most of the examples studied in this paper, the initial timestep size is chosen to allow convergence of the successive iterations and the Newton iterations at the beginning of the process. That is, if we start with a timestep size greater than the initial timesteps chosen here, the non-linear iterations failed to converge after a few time steps.

We performed parametric studies for different values of PID parameters (k_p , k_i , k_D) for two test problems, to verify whether the PID controller is robust or not. Although feedback control theory provides techniques to choose PID parameters, robustness is required when a general method is used for a wide range of different situations. The controller was found to be very robust, allowing us to fix the values of the PID parameters, $k_p = 0.075$, $k_i = 0.175$ and $k_D = 0.01$, for all the numerical experiments performed subsequently. Experimental studies will be given in the next section showing the efficiency of the two controls. Comparative studies between the two controls and the timestep selection strategy suggested by Winget and Hughes [6] will also be carried out for representative test problems. The results with the Winget and Hughes heuristic algorithm will be labelled as W&H.

4. NUMERICAL RESULTS

4.1. Validation problem

Our main objective here is to assess the accuracy of the solutions when the timestep control strategies are applied to a specified problem. We also want to verify whether the PID controller is robust or not. For this investigation, we apply Control 1 to a constructed example with known analytic solution, and we perform parametric studies for different values of PID parameters k_p , k_i and k_D .

Our experiment is a test problem constructed to have in the unit square domain $[0, 1] \times [0, 1]$ and for $t > 0$ the analytic solution

$$c = 10^2(t + 1)^2x(x - 1)y(y - 1) \quad (38)$$

where c is the solution of the transport equation (4) for a single species component. The diffusion tensor is $K_{11} = K_{22} = 1$, $K_{12} = K_{21} = 0$, and the non-linear reaction term is taken to be

$$h_2 = -c^2 + f \quad (39)$$

Table I. Results for Control 1 using bilinear elements on a 2×2 grid.

| Case | k_p, k_I, k_D | error | ntstep | nrejec | newt | c_{effort} |
|------|-------------------|----------------|--------|--------|------|---------------------|
| 1 | 0.05 0.05 0.005 | 0.37023368E-05 | 66 | 0 | 132 | 0.66 |
| 2 | 0.1 0.3 0.015 | 0.38890581E-05 | 62 | 0 | 124 | 0.62 |
| 3 | 0.075 0.175 0.01 | 0.38512072E-05 | 62 | 0 | 124 | 0.62 |
| 4 | 0.1 0.16 0.011 | 0.38680409E-05 | 63 | 0 | 126 | 0.63 |
| 5 | 0.06 0.13 0.008 | 0.38456781E-05 | 63 | 0 | 126 | 0.63 |
| 6 | 0.08 0.216 0.0116 | 0.38684855E-05 | 62 | 0 | 124 | 0.62 |
| 7 | 0.15 0.32 0.017 | 0.38897674E-05 | 62 | 1 | 126 | 0.63 |
| 8 | 0.2 0.4 0.02 | 0.38896720E-05 | 62 | 2 | 128 | 0.64 |
| 9 | 0.04 0.04 0.004 | 0.36271440E-05 | 67 | 0 | 134 | 0.67 |
| 10 | 0.03 0.03 0.003 | 0.35057604E-05 | 69 | 0 | 138 | 0.69 |
| 11 | 0.0 0.175 0.0 | 0.38528566E-05 | 62 | 0 | 124 | 0.62 |
| 12 | 0.075 0.175 0.0 | 0.38512100E-05 | 62 | 0 | 124 | 0.62 |
| 13 | Fixed Δt | 0.13711077E-05 | 100 | 0 | 200 | 1 |

where the function f is given by

$$f = \frac{\partial c}{\partial t} + u \frac{\partial c}{\partial x} + v \frac{\partial c}{\partial y} - K_{11} \frac{\partial^2 c}{\partial x^2} - K_{22} \frac{\partial^2 c}{\partial y^2} + c^2 \quad (40)$$

The initial solution is defined as the exact solution at the initial time $t = 0$. We specify essential boundary conditions similarly and the exact velocity field is taken to be

$$\begin{aligned} u(t, x, y) &= (t + 1)^2 x^2 (1 - x)^2 (2y - 6y^2 + 4y^3) \\ v(t, x, y) &= (t + 1)^2 y^2 (1 - y)^2 (-2x + 6x^2 - 4x^3) \end{aligned} \quad (41)$$

This velocity field is divergence free and satisfies the no-slip condition $\mathbf{u} = \mathbf{0}$ on the boundary of the square. The maximum nodal velocity is approximately 1.2×10^{-2} , which corresponds to a Reynolds number of $Re = 1.2$.

We use in these experiments a 2×2 grid with biquadratic elements, since the relative errors in the L^2 -norm for any number of elements is within roundoff error. The initial timestep size is 10^{-4} , and we allow minimum and maximum timestep sizes of 10^{-4} and 10^{-3} , respectively. Changes in nodal concentration are calculated with an input tolerance of 10^{-5} , and the calculations stop when the time is greater than 0.01. We perform parametric studies of the timestep controller for values similar to those used by Gustafsson *et al.* [9] and also by Coutinho and Alves [27]. We choose values of k_p ranging from 0.03 to 0.20, k_I from 0.03 to 0.40, and k_D from 0.003 to 0.02. We also study the case where $k_p = k_D = 0$.

Table I shows the L^2 -norm of the error in the concentration solution, the number of time iterations, ntstep, the number of rejected steps, nrejec, the total number of Newton iterations, newt, and the computational effort, c_{effort} , defined here as newt divided by the number of Newton iterations obtained using a fixed timestep size of 10^{-4} . We can see from Table I that the error in the approximate solution at the final time is of order 10^{-6} for all cases studied. Moreover, with the PID control strategy we find approximate solutions with a smaller number of time steps without any significant loss of accuracy.

The PID controller is very robust as we can also see from Table I. Although feedback control theory provides techniques to choose the PID parameters, robustness is required when

a general finite element method is used for a wide range of different simulations. The variation in the number of time iterations is very small if we keep k_p in the range 0.03 to 0.20, k_i from 0.03 to 0.40, and k_D from 0.003 to 0.02. For these reasons, we fix the values of the PID parameters equal to $k_p = 0.075$, $k_i = 0.175$ and $k_D = 0.01$ in all the numerical experiments performed subsequently. In most cases, a PI controller is satisfactory. However, we show that these values are also suitable for the other application problems presented here, and we see more significant improvements with the new adaptive schemes in these latter applications.

4.2. Rayleigh–Benard–Marangoni problems

Natural convection of an incompressible fluid can be driven by buoyancy forces due to temperature gradients and thermocapillary forces caused by gradients in the surface tension [28–31]. The classic Rayleigh–Benard problem corresponds to flow between two horizontal plates where the top plate is held at a constant (cool) temperature and the bottom plate is held at a higher constant temperature. At critical Rayleigh number the heated fluid near the bottom plate begins to rise while the (cool) fluid near the top is more dense and descends. This leads to circular convection cells in two dimensions. If the plate is removed from the upper surface, then the thermocapillary surface tension due to temperature gradients on the free surface also becomes important. This is a direct consequence of the dependence of surface tension on temperature (Marangoni effect). Now, both buoyancy and thermocapillary effects may be important in driving the flow for this classical Rayleigh–Benard–Marangoni problem.

The dimensionless equations describing Rayleigh–Benard–Marangoni flows are

$$\frac{\partial \mathbf{u}}{\partial t} + \mathbf{u} \cdot \nabla \mathbf{u} - \nabla^2 \mathbf{u} + \nabla p = \frac{Ra}{Pr} T \mathbf{g} \quad \text{in } \Omega \times I \quad (42)$$

$$\nabla \cdot \mathbf{u} = 0 \quad \text{in } \Omega \times I \quad (43)$$

$$\frac{\partial T}{\partial t} + \mathbf{u} \cdot \nabla T - \frac{1}{Pr} \nabla^2 T = 0 \quad \text{in } \Omega \times I \quad (44)$$

where Ω is the domain, $I = [0, \bar{t}]$ the time interval, $Ra = \beta_T \Delta T g L^3 / \nu \alpha$ the Rayleigh number, $Pr = \nu / \alpha$ the Prandtl number, β_T the thermal coefficient, g the gravity, ν the kinematic viscosity, $\alpha = k / \rho c_p$ the thermal diffusivity, k the thermal conductivity, ρ the density, and c_p the specific heat.

We assume that there is no slip at the solid walls $\partial\Omega_1$, i.e. $\mathbf{u} = \mathbf{u}_w$ where \mathbf{u}_w is the specified wall boundary velocity. Temperature, flux or mixed thermal boundary conditions may be applied. The Marangoni problem involves a shear stress boundary in the free surface $\partial\Omega_2$. The boundary condition on the free surface is

$$\nabla \mathbf{u} \cdot \mathbf{n} = -\frac{Ma}{Pr} \nabla T \cdot \mathbf{t} \quad (45)$$

where $Ma = \sigma_T \Delta T L / \rho \nu \alpha$ is the Marangoni number, $\sigma_T = \partial\sigma / \partial T$ is determined empirically for a given fluid, \mathbf{n} is unit normal vector, and \mathbf{t} is a unit tangent vector. Here we assume that surface tension σ varies linearly with T , so σ_T is a constant for a given fluid.

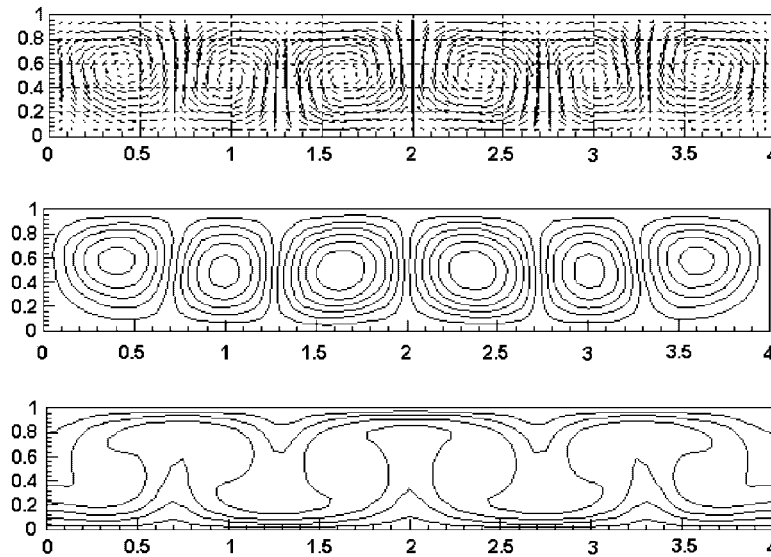


Figure 3. Vector field, streamlines, and temperature contours for flow in a container with aspect ratio 4:1

Table II. Computational effort for flow in a container with aspect ratio 4:1.

| | ntstep | nrejec | nsa | C_{effort} |
|------------------|--------|--------|-----|---------------------|
| Fixed Δt | 241 | 0 | 731 | 1 |
| Control 1 | 192 | 0 | 643 | 0.88 |
| Control 2 | 89 | 1 | 380 | 0.52 |
| W&H | 193 | 0 | 644 | 0.88 |

We investigate the formation of Rayleigh–Benard cells treating the flow in a two-dimensional simulation. We consider the flow in a rectangular container with aspect ratio 4:1 (length:width), insulated lateral walls, $Pr = 0.72$ and $Ra = 30\,000$. Temperatures on bottom and top surfaces are normalized to $T = 1$ and 0 , respectively. The initial conditions are $\mathbf{u} = 0$ and $T(x, y) = 1 - y$ in the domain. The approximate velocity and temperature are calculated using biquadratic shape functions with a grid of 32×8 elements, and the control algorithms for timestep selection. We approach steady state using fixed and adapted timesteps. The resulting velocity field, streamlines and temperature contours are shown in Figure 3. There are six recirculation cells, and the results agree well with those obtained by Griebel *et al.* [32].

Table II shows the computational effort for this problem, measured by the total number of successive approximations needed to calculate the velocity field using one of the approaches divided by the number of successive approximations obtained using a fixed timestep size. For each case, we calculate the number of time iterations, ntstep, the number of rejected steps, nrejec, the total number of successive approximations, nsa, and the computational effort, C_{effort} . We start with a timestep size of 0.001, and we allow minimum and maximum time steps of 0.001 and 0.5, respectively. We set a tolerance of 0.01 for changes in nodal velocities and

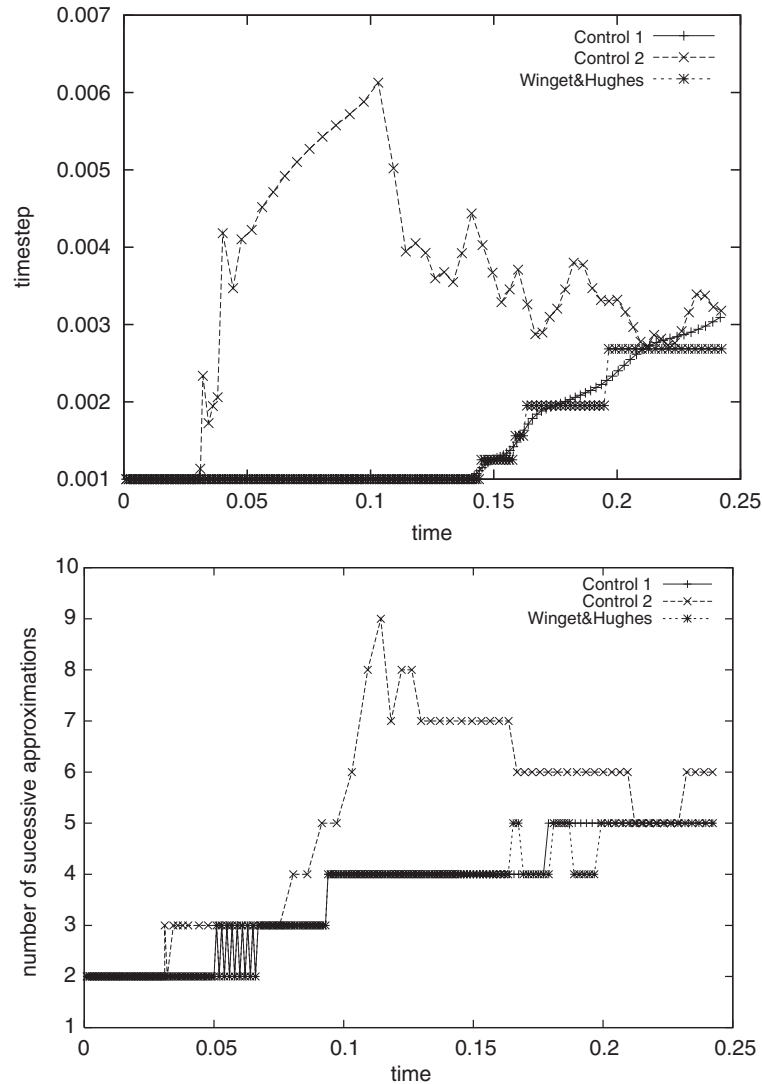


Figure 4. Timestep variation (top) and number of successive approximations (bottom) using Control 1, Control 2 and W&H for the flow in a container with aspect ratio 4:1.

temperature and 0.8 for changes in the kinetic energy. The reference rate of convergence for Control 2 is 0.35 in this example.

As we can see in Table II, we obtain solutions with a reduced number of successive approximation iterations using all the controllers. However, Control 2 gives the smallest computational effort. With a fixed timestep size of 0.001 we need 731 iterations, and only 380 iterations when Control 2 is applied. Thus, the solution is obtained 1.9 times faster using Control 2. In this example, Control 1 and W&H are equivalent in terms of computational

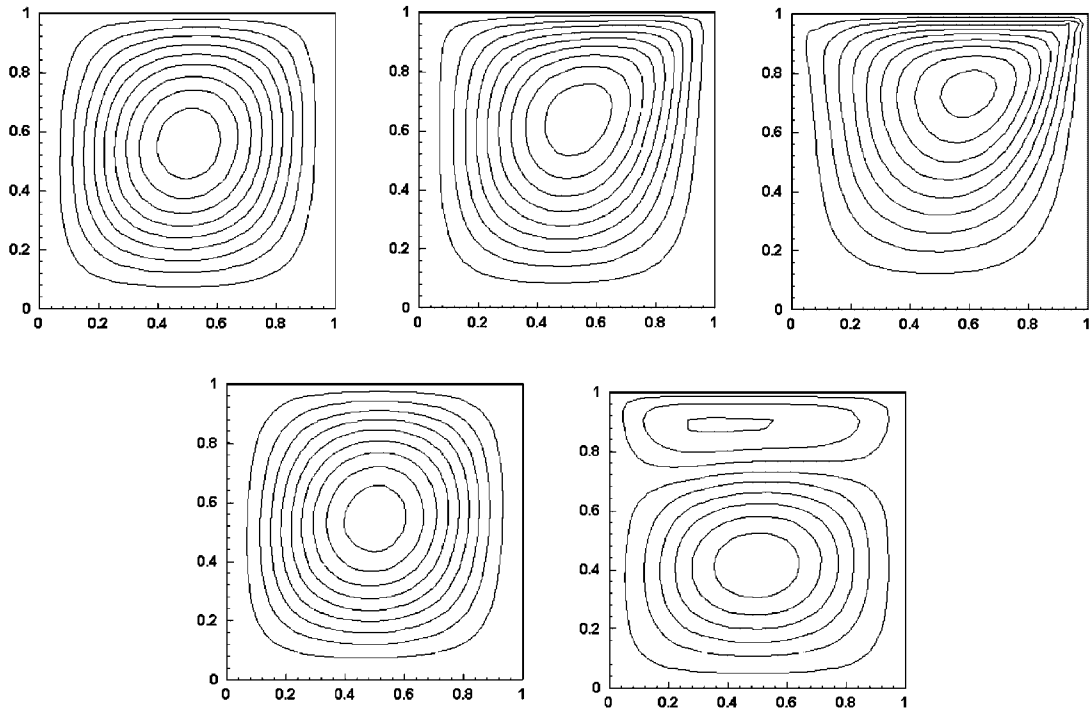


Figure 5. Stream function contours for $Ma = 1$, $Ma = 100$, $Ma = 1000$ (top) and $Ma = -10$, $Ma = -100$ (bottom).

effort. Figure 4 shows the timestep size against time and the number of successive approximation iterations using Control 1, Control 2 and W&H. We see that Control 2 produces bigger timesteps with a moderate increase in the number of successive iterations.

The second experiment involves buoyancy forces due to temperature gradients and thermocapillary forces caused by gradients in the surface tension. The flow domain is a unit square $\Omega = [0, 1] \times [0, 1]$ with temperatures $T = 1$, $T = 0$ on the left and right walls, respectively, adiabatic bottom wall and the top is a flat free surface. The initial conditions are $\mathbf{u} = \mathbf{0}$ and $T(x, y) = 1 - x$ in the domain. The approximate steady-state velocities and temperature are calculated using biquadratic elements in a uniform mesh with 16×16 elements. The Rayleigh number is 10^3 , the Prandtl number is $Pr = 0.71$, and the problem is solved at $Ma = 1$, 100 and 1000 (see Figure 5). At $Ma = 1$, the effect of the surface tension is small and the streamlines are roughly circular. The solution is similar in structure to the classic buoyancy driven flow. At $Ma = 100$, the effect of the thermocapillary force at the free surface is more pronounced. The streamlines are concentrated near the top boundary. At $Ma = 1000$, the flow is being strongly driven at the top boundary as seen in similar experiments presented by Zebib *et al.* [31]. We consider also the case of a fluid where the surface tension acts in the direction contrary to the thermal gradient. Similar situations arise for fluids in welding when impurities are presented [33]. Figure 5 shows the stream function contours for $Ma = -10$ and -100 . The contours at $Ma = -10$ look similar to the solution at $Ma = 1$ due to the small

Table III. Computational effort for the Rayleigh–Benard–Marangoni problem, $Pr = 0.71$, $Ra=1000$ and $Ma = 100$ in a unit square.

| Case | ntstep | nrejec | nsa | C_{effort} |
|------------------|--------|--------|-----|---------------------|
| Fixed Δt | 118 | 0 | 272 | 1 |
| Control 1 | 23 | 0 | 75 | 0.28 |
| Control 2 | 13 | 0 | 57 | 0.21 |
| W&H | 25 | 0 | 80 | 0.29 |

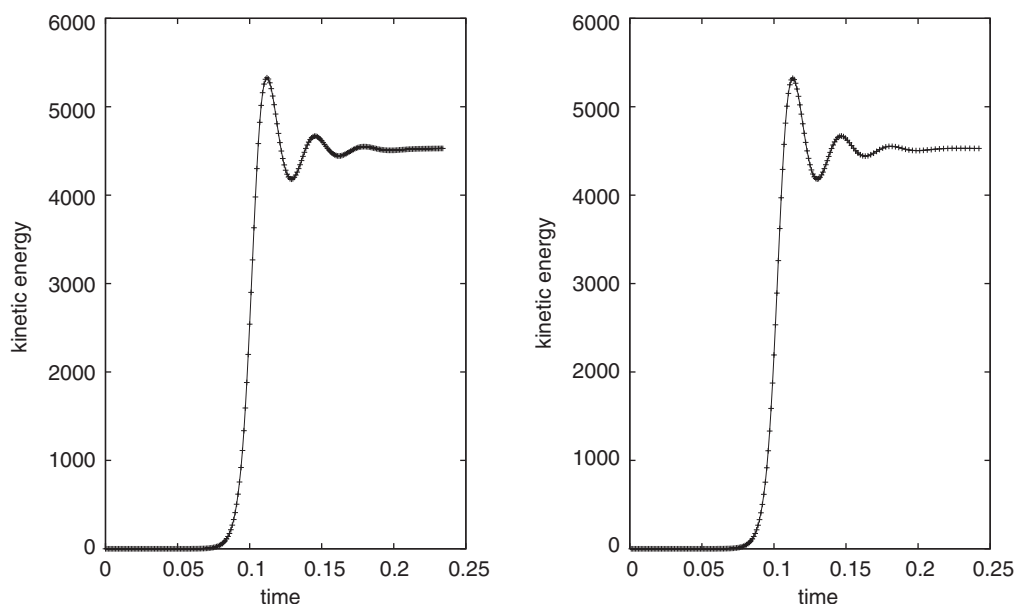


Figure 6. Non-dimensional kinetic energy plotted as a function of time calculated using fixed timestep sizes of 0.001 (left) and using Control 1 (right).

thermocapillary effect. At $Ma = -100$, the surface tension effect is strong enough to reverse the flow on the top surface and two cells are formed.

To study the behaviour of the PID timestep selection algorithms, we select the case where $Ma = 100$. We start with a minimum timestep size of 0.001, and we allow a maximum timestep of 0.1. Solutions are obtained with tolerances of 0.2 and 0.1 for changes in nodal velocities and temperature, respectively. The tolerance corresponding to the normalized changes in kinetic energy is equal to one. The reference rate of convergence is equal to 0.2. As we can see in Table III, we obtain the solutions with 57 successive approximation iterations using Control 2. With a fixed timestep size of 0.001, we need 272 iterations. Thus, the solutions are obtained 4.8 times faster using Control 2. Here, the choice of the timestep in Control 2 is dominated by the changes in the kinetic energy, with only three time iterations limited by the changes in the convergence rate of the successive iterations. Figure 6 shows the time evolution of the non-dimensional kinetic energy calculated using fixed timestep sizes of 0.001 and using Control 1.

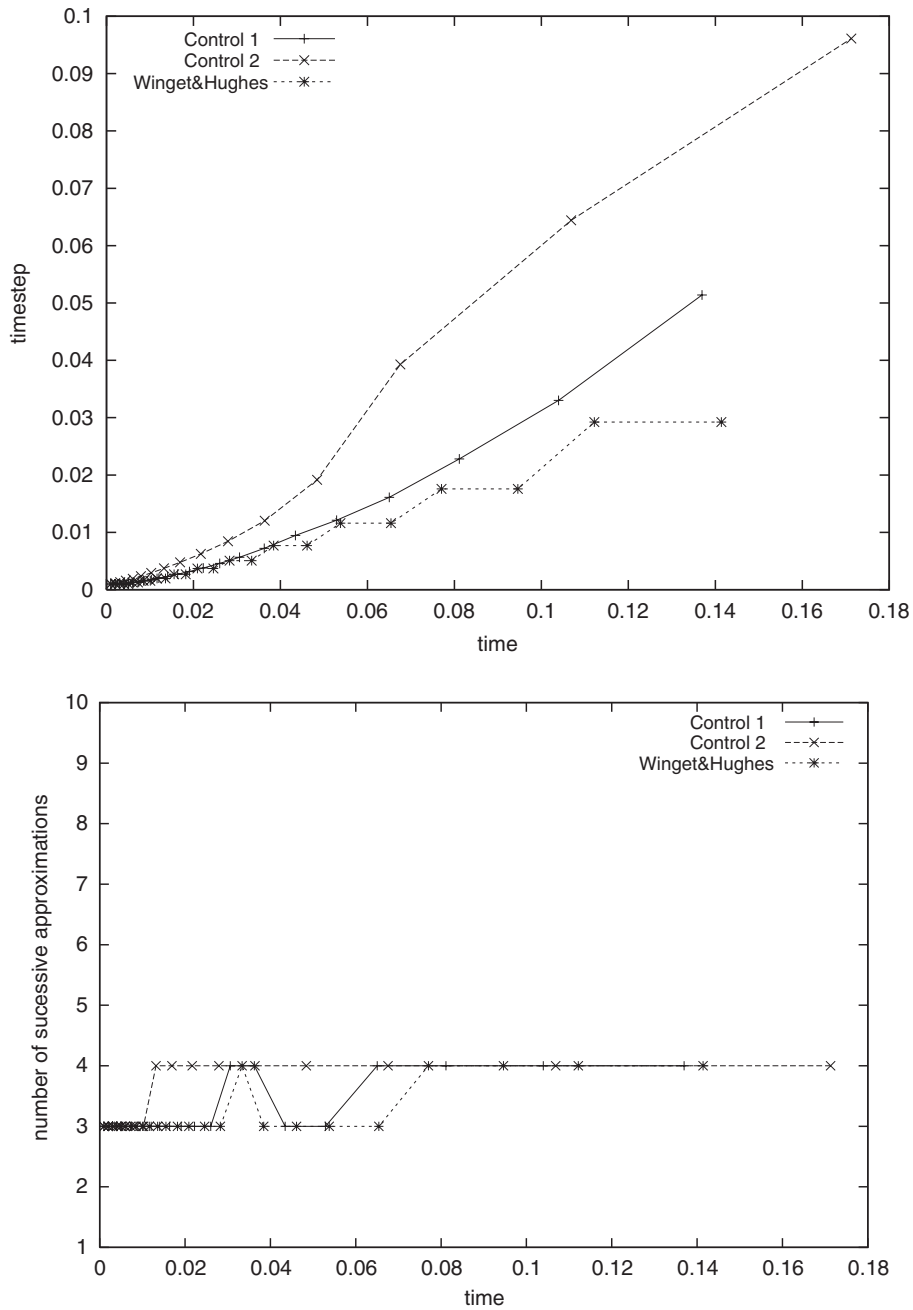


Figure 7. Timestep variation (top) and number of successive approximations (bottom) using Control 1, Control 2 and W&H for $Pr = 0.71$, $Ra=1000$ and $Ma = 100$ in a unit square.

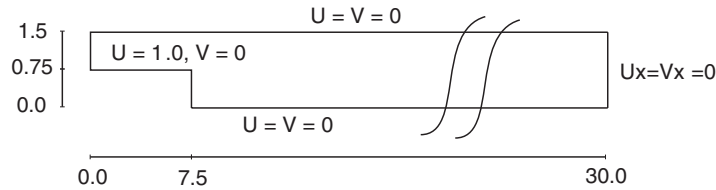


Figure 8. Backward-facing step geometry with channel dimensions and boundary conditions.

Figure 7 shows the timestep variation and the number of successive approximations against time using Control 1, Control 2 and W&H, respectively. We observe that Control 1 yields a smoother sequence of time steps than W&H. However, these two approaches are equivalent in terms of efficiency. Control 2 calculates the solution with the smallest computational effort.

4.3. Flow over a backward-facing step

The next experiment is for the backward-facing step problem, Figure 8. Results of physical experiments are given in Reference [34], and numerical results obtained using different finite element methods can be found, for example, in References [35,36]. In Reference [32] the problem is solved for different Reynolds numbers using a finite difference approach. Numerical results using our penalty finite element formulation are compared with those published by Griebel *et al.* [32].

The problem involves viscous incompressible flow over an isothermal two-dimensional backward-facing step. Introducing the dimensionless variables $x^* = x/L$, $y^* = y/L$, $t^* = tu_\infty/L$, $u^* = u/u_\infty$, $v^* = v/v_\infty$, $p^* = (p - p_\infty)/\rho_\infty u_\infty^2$, with given scalar constants L , u_∞ , p_∞ , ρ_∞ , and substituting these relations into (1) and (5), we obtain

$$\frac{\partial \mathbf{u}}{\partial t} + \mathbf{u} \cdot \nabla \mathbf{u} - \frac{1}{Re} \Delta \mathbf{u} + \nabla p = \mathbf{0} \quad \text{in } \Omega \times I \quad (46)$$

$$\nabla \cdot \mathbf{u} = 0 \quad \text{in } \Omega \times I \quad (47)$$

where we have dropped the superscript $*$ for simplicity, and $Re = \rho_\infty u_\infty L / \mu$ is the Reynolds number. The initial velocity is $u = 1.0$, $v = 0$ in the upper half of the domain and $u = v = 0$ in the lower half. The step is the rectangle $[0, 7.5] \times [0, 0.75]$ and the inflow velocity at the left end has the constant value $u = 1.0$. The length L measured from the step to the end of the calculation domain was selected to make the reattachment length independent of the calculation domain, and the boundary condition at the outflow section was taken as that of a fully developed flow. We solve the problem towards steady state for Reynolds numbers, $Re = 100$ and 500 .

The mesh is uniform for $0 \leq x \leq 15$ with $(\Delta x, \Delta y) = (0.1875, 0.3)$. For the downstream region $15 \leq x \leq 30$ and $0 \leq y \leq 1.5$ the mesh is uniform across the channel but smoothly graded in the flow direction using

$$x(i) = 15 + 15 * \left(\frac{i-1}{nx-1} \right)^{1.2} \quad (48)$$

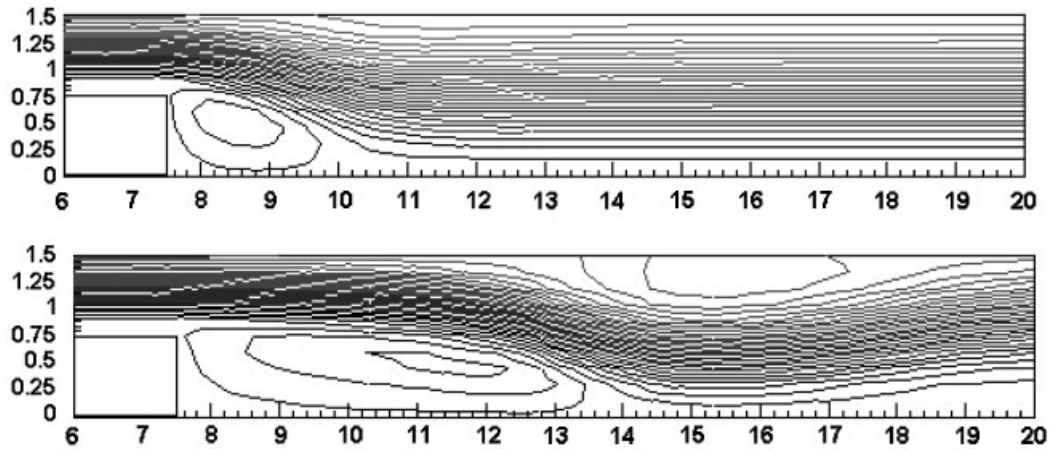


Figure 9. Flow over a backward-facing step, streamlines at $Re = 100$ (top) and $Re = 500$ (bottom).

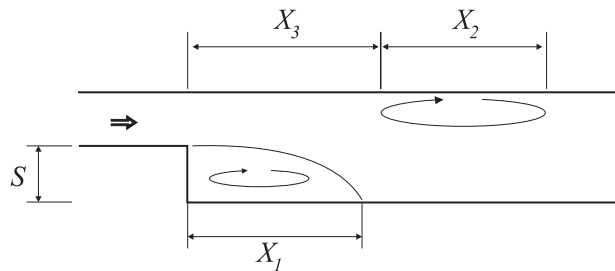


Figure 10. Characteristic lengths.

where $nx = 30$ is the number of elements in the downstream region. Elements near $x = 30$ are approximately twice the length of elements near $x = 15$. The steady-state solution is approached when $\|\mathbf{u}^n - \mathbf{u}^{n-1}\| < 10^{-7} \|\mathbf{u}^n\|$. Results were obtained using the four-node continuous bilinear velocity element with 1-point Gauss quadrature for the penalty term.

The basic character of the backward-facing step flow at $Re = 100$ and 500 is well known and is illustrated in the contour plots of Figure 9. Note that the figures show only the part of the computational domain $6 \leq x \leq 20$, since this contains all the essential features. The streamlines shown in Figure 9 reveal that, for $Re = 100$, the flow widens immediately behind the step and an eddy of moderate size is evident behind the step. When viscosity is further reduced ($Re = 500$), the main flow is drawn downward, causing it to separate from the upper boundary and leading to the formation of a second eddy. Note that the first eddy increases in size with increasing Reynolds number ($Re = 500$).

The lengths X_1 and X_2 of the lower and upper eddies as well the horizontal distance X_3 from the step to the upper eddy's point of separation are values often used to characterize the resulting flow, see Figure 10. For $Re = 100$, we can observe in Figure 9 that the flow

Table IV. Computational effort for the backward-facing step flow at $Re = 100$.

| $Re = 100$ | ntstep | nrejec | nsa | C_{effort} |
|------------------|--------|--------|------|---------------------|
| Fixed Δt | 1094 | 0 | 3236 | 1 |
| Control 1 | 46 | 0 | 320 | 0.10 |
| Control 2 | 63 | 0 | 375 | 0.12 |
| W&H | 59 | 0 | 370 | 0.11 |
| H211PI | 42 | 0 | 298 | 0.09 |

separates at the step corner and forms a recirculation eddy with a reattachment point on the lower wall approximately at $x = 10.35$ which corresponds to $X_1 = 2.85$. This eddy increases in size to $x = 13.725$ ($X_1 = 6.225$) with increasing Reynolds number ($Re = 500$). A second eddy forms on the upper wall, for $Re = 500$, beginning approximately at $x = 12.15$ and terminating at $x = 18.975$ ($X_2 = 6.825$ and $X_3 = 4.65$). The results are in exact agreement with the results reported by Griebel *et al.* [32].

Now we compare the computational effort to calculate the solution for $Re = 100$ in Table IV. In this case, we also implemented the PI controller suggested by Söderlind [19] known as H211PI. The PI controller and first-order digital filter has a negative proportional gain ($k_p < 0$) and is given by

$$\Delta t_{n+1} = \left(\frac{1}{e_n}\right)^{k_i+k_p} \left(\frac{1}{e_{n-1}}\right)^{-k_p} \Delta t_n \quad (49)$$

with parameters $k_i = 1/3$, $k_p = -1/6$ and $k_D = 0$. We start with a timestep size of 0.02, and we allow minimum and maximum time steps of 0.02 and 1.0, respectively. The solutions are obtained with a tolerance of 10^{-3} for changes in nodal velocities. The tolerance corresponding to the normalized changes in kinetic energy is equal to 0.1, and the reference rate of convergence is equal to 0.25. We allowed a maximum number of successive approximations, nsa_{max} , equal to 10. As we can see in Table IV, we obtain the solutions with a reduced number of successive approximation iterations in all cases, and the controllers are equivalent in terms of efficiency. The choice of the timestep in Control 2 is dominated by the convergence rate of the successive iterations, with only 15 timesteps limited by the changes in the kinetic energy. Figure 11 shows the timestep variation and the number of successive approximations against time using Control 1, Control 2, W&H and H211PI, respectively. Observe that Control 1 and H211PI controller have a similar behaviour and produce a very smooth curve, while W&H yields a curve with several steps and Control 2 oscillates tremendously. In our experiments, if the step size is bigger than the maximum time step allowed, $\Delta t_{\text{max}} = 1$, the number of successive approximations obtained is bigger than the maximum number of successive approximations allowed, $nsa_{\text{max}} = 10$. As a consequence, we can observe that at the end of the process, the timestep sizes are kept equal to the maximum size allowed.

Next, we compare the computational effort to calculate the solution for $Re=500$ in Table V. We start with a timestep size of 0.02, and we allow minimum and maximum time steps of 0.02 and 1.0, respectively. The solutions are obtained with a tolerance of 10^{-4} for changes in nodal velocities. The tolerance corresponding to the normalized changes in kinetic energy

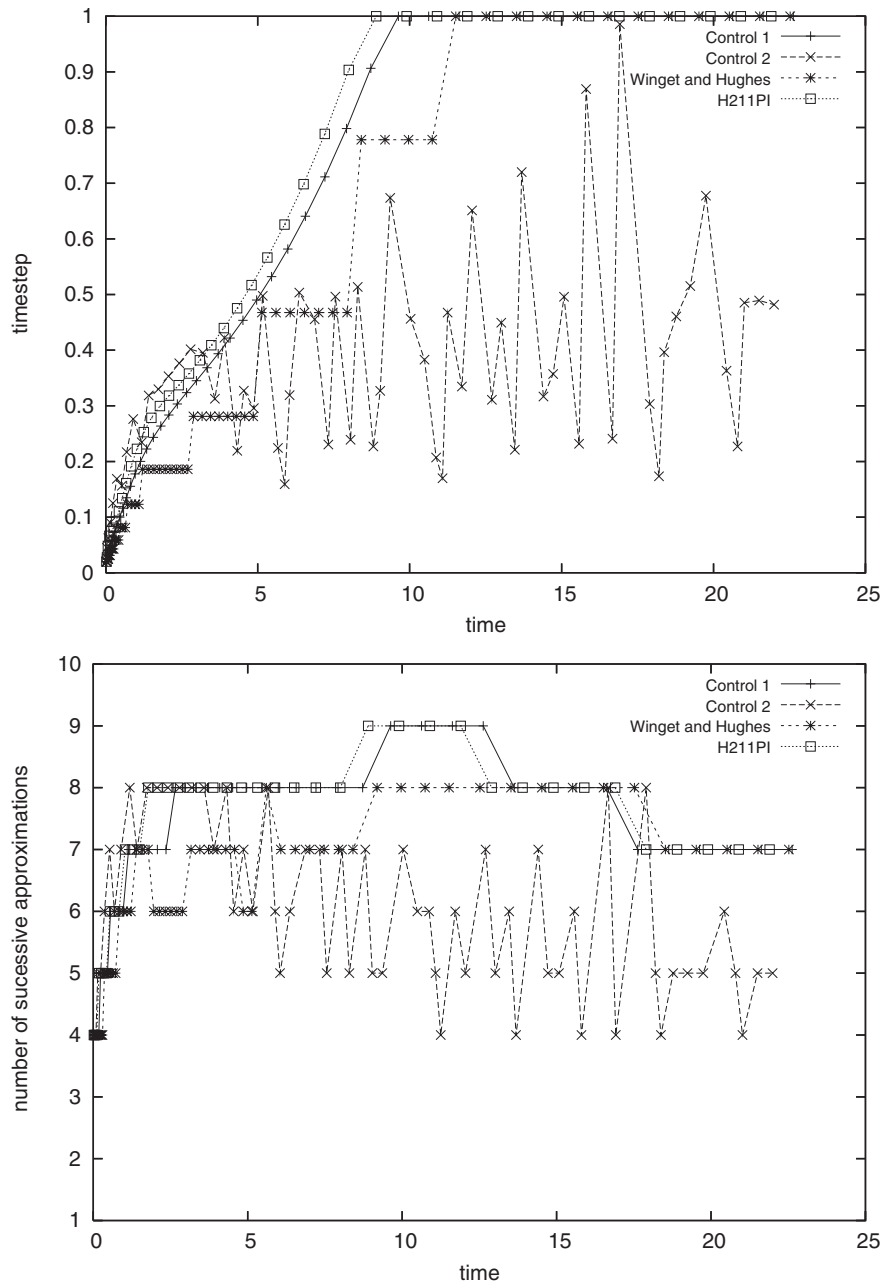


Figure 11. Timestep variation (top) and number of successive approximations (bottom) using Control 1, Control 2, W&H and H211PI for $Re = 100$.

Table V. Computational effort for the backward-facing step flow at $Re = 500$.

| $Re = 500$ | ntstep | nrejec | nsa | C_{effort} |
|------------------|--------|--------|------|---------------------|
| Fixed Δt | 1628 | 0 | 5916 | 1 |
| Control 1 | 283 | 0 | 1477 | 0.25 |
| Control 2 | 183 | 0 | 1164 | 0.20 |
| W&H | 436 | 1 | 2189 | 0.37 |

is equal to 0.01, and the reference rate of convergence is equal to 0.2. As we can see in Table V, Control 2 gives the smallest computational effort. With a fixed timestep size of 0.02 we need 5916 iterations, and only 1164 iterations when Control 2 is applied. Thus, the solution is obtained 5 times faster using Control 2. The choice of the timestep in Control 2 is dominated by the convergence rate of the successive iterations, with 61 timesteps limited by the changes in the kinetic energy. Figure 12 shows the timestep variation and the number of successive approximations against time using Control 1, Control 2 and W&H, respectively. We can observe that Control 1 yields a smoother sequence of timesteps than W&H, and Control 2 oscillates wildly in this example. Since the size of the timestep increases at the beginning of the process for Control 1 and W&H, the number of successive iterations to obtain convergence of the non-linear process at each corresponding time also increases. The oscillatory behaviour of Control 2 is responsible for the large variation of the number of successive iterations calculated by this controller.

4.4. Flow past a circular cylinder

Flow past a circular cylinder has become a traditional benchmark problem used to test the performance of various numerical methods [22, 37, 38]. The flow around a stationary cylinder presents many varied physical characteristics depending on Reynolds number. For a Reynolds number based on the free stream velocity and on the cylinder diameter, experiments show that a steady-state solution with symmetric attached recirculation regions occurs up to Reynolds numbers equal to 40. However, for higher Reynolds numbers, the flow shows a periodic shedding of vortices, forming what is called a Von Karmann vortex street.

The geometry and boundary conditions considered are depicted in Figure 13. The diameter of the cylinder is one, and free traction boundary conditions are imposed at the outflow section. The initial condition consists of a uniform velocity field with $u = 1$ everywhere, except along the cylinder surface, where non-slip conditions have been assumed. Figure 14 shows the mesh, containing 4683 nodes and 4520 elements.

We solve the problem using our control algorithms to obtain the approximate solutions, and compare our results with those obtained by Engelman and Jamnia [37]. In their work, they used a variable-time-increment approach based on controlling the local time truncation error at each step. The variable time increment settled down to a constant increment of 0.269 after 100 time steps. This results in about 22 timesteps for each vortex shedding cycle. In our control algorithms, we allowed a minimum timestep size of 0.05 and a maximum timestep size of 0.3. In this example, Control 1 uses the changes in nodal vertical velocity component at point q .

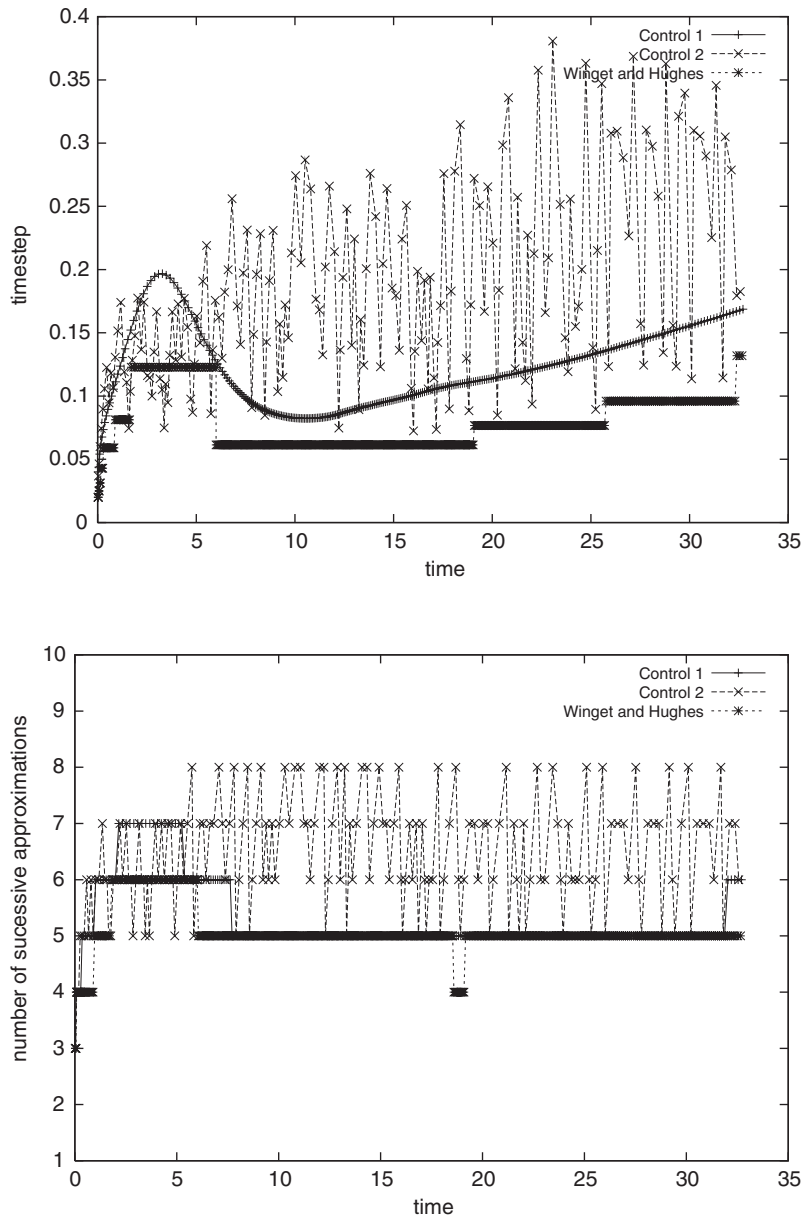


Figure 12. Timestep variation (top) and number of successive approximations (bottom) using Control 1, Control 2 and W&H for $Re = 500$.

The variation of the vertical velocity component v at point q is shown in Figure 15 for the two control approaches from $t = 60$ to $t = 180$. Note that after an initial transient, the vertical velocity component v exhibits a periodic behaviour. Vortices begin to shed after approximately

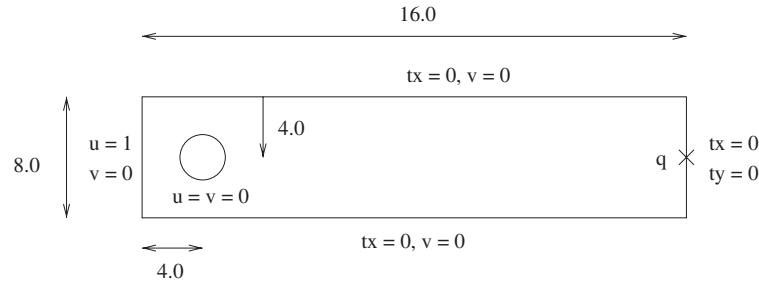


Figure 13. Domain specification and boundary conditions for the cylinder in a crossflow problem.

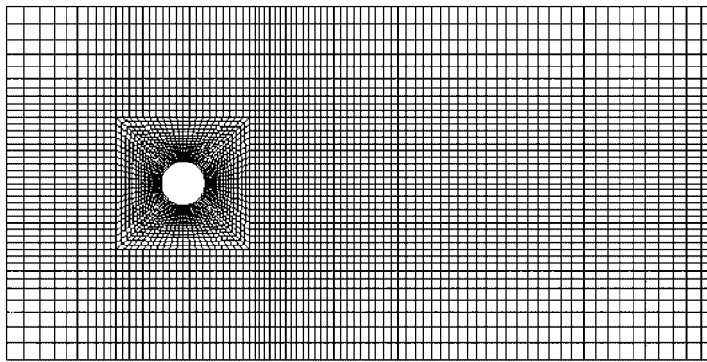


Figure 14. Finite element mesh with 4683 nodes and 4520 elements.

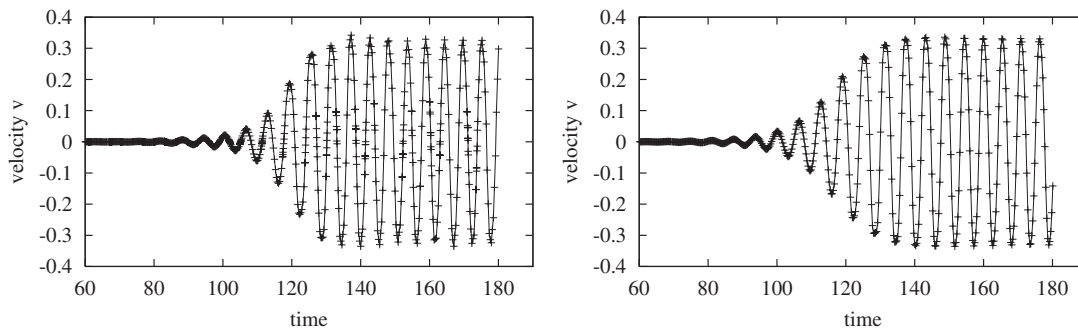


Figure 15. Flow past a circular cylinder, vertical velocity component at point q using Control 1 (left) and Control 2 (right).

100 timesteps and by timestep 150 the periodic vortex street is well established. The time histories at location q for the vertical velocity component v is in accordance with the results presented in Reference [37]. A typical velocity field vector plot for $Re = 100$ is given in Figure 16.

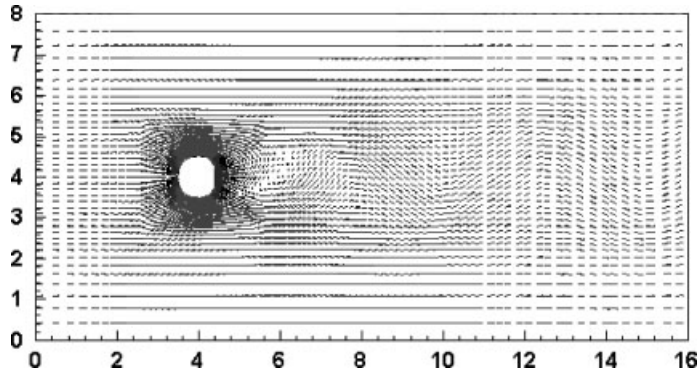


Figure 16. Vector plot at $t = 160$, $Re = 100$, obtained with $\Delta t = 0.05$.

Table VI. Computational effort for the transient flow past a circular cylinder, $Ra = 100$.

| Case | ntstep | nrejec | nsa | C_{effort} |
|------------------|--------|--------|-------|---------------------|
| Fixed Δt | 3600 | 0 | 18007 | 1 |
| Control 1 | 844 | 126 | 7726 | 0.43 |
| Control 2 | 623 | 0 | 4974 | 0.28 |

Of particular interest for the vortex-shedding problem are the period τ for one shedding cycle and the Strouhal number $St = Df/v$, where $f = 1/\tau$ is the shedding frequency, D is cylinder diameter, and v is the horizontal velocity component. These values are $\tau = 5.4$, $St = 0.185$ for Control 1 and $\tau = 5.8$, $St = 0.173$ for Control 2. The numerical results obtained using Control 2 are in exact agreement with the available data in Reference [37]. To provide good temporal resolution, it is necessary to take at least 100 timesteps per period. However, as we want to verify the performance of our control algorithms and compare with numerical data available in the literature, we allowed a maximum time step size of 0.3, which corresponds to 20 timesteps per shedding cycle. The Strouhal numbers above differ from experiments, $St_{\text{exp}} = 0.167$, in [22]. This may be a consequence of an inappropriate choice of the spatial domain for the model problem and the small number of timesteps per vortex shedding.

The computational effort to obtain the numerical solutions for the flow past a circular cylinder problem is shown in Table VI for $t = [0, 180]$. For Control 1, we decided to control the fluid movement at point q at the outflow boundary. We define a tolerance of 3.0 for changes in the vertical velocity component at this point. For Control 2, the successive changes in kinetic energy are limited to 10.0, and the reference rate of convergence is equal to 0.3. The controllers reduce the number of successive approximations necessary to calculate the approximations, and Control 2 presents the best results.

The variation in timestep sizes is shown in Figure 17. Control 2 keeps the timestep size close to the maximum value while Control 1 varies the timestep size between the minimum and the maximum values. This is probably the justification for the superior performance of Control 2. After two initial timesteps, the number of successive approximations necessary for

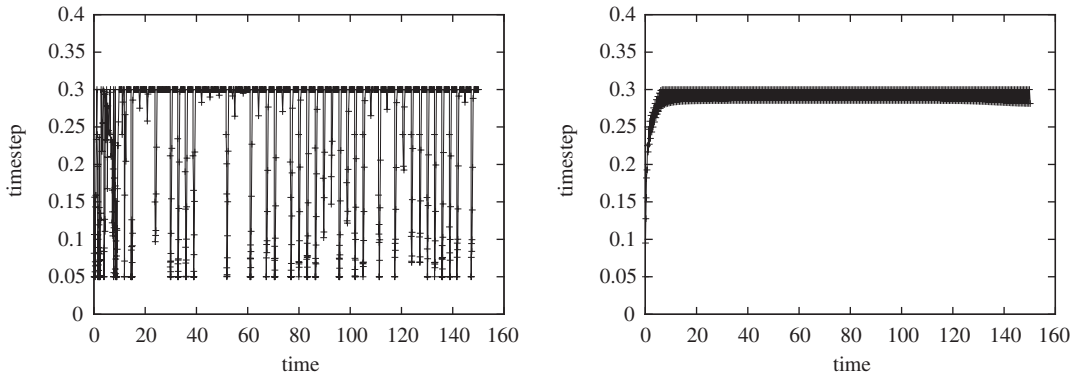


Figure 17. Timestep variation using Control 1 (left) and Control 2 (right) the transient flow past a circular cylinder problem, $Ra = 100$.

convergence of the non-linear process at each timestep size remains fixed at 8 for Control 2. For Control 1, the number of successive approximations varies between 5 and 8.

4.5. Chemical reaction systems

The last class of problems studied here involves non-linear flow and reactive transport. We solve chemical reaction on a catalyst section with heat effects included [39, 40]. The process is highly non-linear because of an exponential chemical reaction term arising from the temperature dependence of the chemical reaction rate. As a consequence, we need to choose a very small timestep to obtain convergence of the non-linear iterations in the transport equation. Therefore, efficient computation of the transport process in this example demands the use of timestep selection algorithms.

When a domain or body made from a porous material impregnated with a catalytic substance is submerged in a gas stream, the reactant A diffuses into the domain or body, reacts on the catalytic surface, and the product B diffuses out. We assume that the process $A \rightarrow B$ is non-isothermal and homogeneous and that the chemical change takes place in the entire volume of the fluid. We also assume that the reaction mechanism is known [40, 41]. Consider a first-order, irreversible reaction in a catalyst section $[-L, L] \times [-L, L]$ with reaction rate given by $R = -ac \exp(-\Delta E/\hat{R}T)$, where T is the absolute temperature, ΔE is the activation energy, \hat{R} is the gas constant, and a is constant.

The dimensionless unsteady equations for the non-isothermal problem are

$$\frac{\partial T}{\partial t} + \mathbf{u} \cdot \nabla T - \frac{1}{M_1} \nabla^2 T = \frac{\phi^2 c \beta}{M_1} \exp\left(\gamma \left(1 - \frac{1}{T}\right)\right) \quad (50)$$

$$\frac{\partial c}{\partial t} + \mathbf{u} \cdot \nabla c - \frac{1}{M_2} \nabla^2 c = -\frac{\phi^2 c}{M_2} \exp\left(\gamma \left(1 - \frac{1}{T}\right)\right) \quad (51)$$

with initial conditions

$$T(x, y, 0) = c(x, y, 0) = 1 + \sin(\pi x) \sin(\pi y) \quad (52)$$

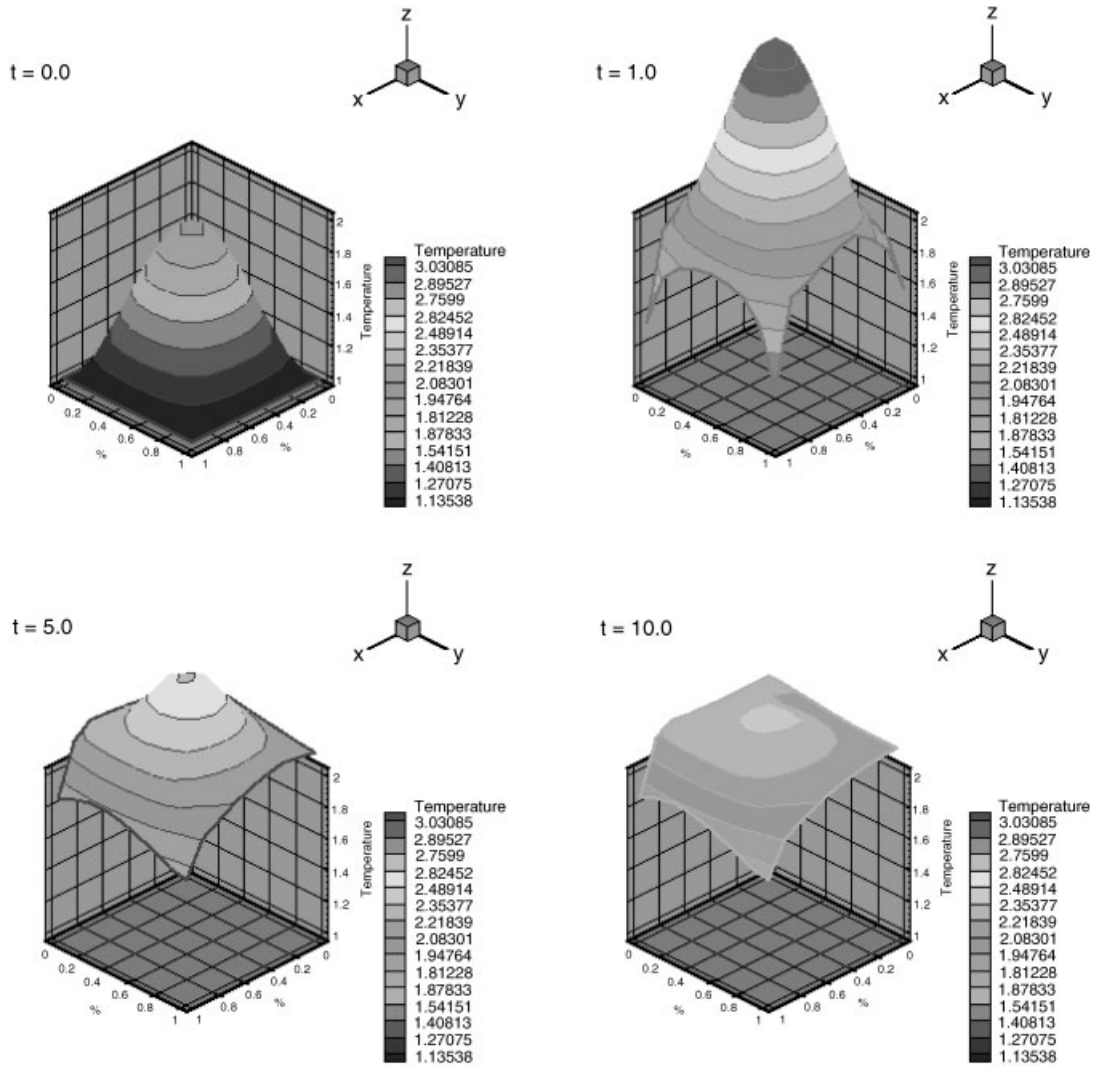


Figure 18. Evolution of temperature solution using bilinear elements on a 8×8 grid for the non-isothermal problem.

and boundary conditions

$$\nabla T \cdot \mathbf{n} = \nabla c \cdot \mathbf{n} = 0 \quad \text{on } \partial\Omega_1$$

$$-\nabla T \cdot \mathbf{n} = \frac{Nu}{2}(T - 1.1) \quad \text{on } \partial\Omega_2 \tag{53}$$

$$-\nabla c \cdot \mathbf{n} = \frac{Sh}{2}(c - 1.0) \quad \text{on } \partial\Omega_2 \tag{54}$$

Table VII. Results with Control 1 and W&H for the non-isothermal problem.

| Case | ntstep | nrejec | newt | c_{effort} |
|------------|--------|--------|------|---------------------|
| No control | 400 | 0 | 1223 | 1 |
| Control 1 | 104 | 1 | 423 | 0.34 |
| W&H | 112 | 1 | 433 | 0.35 |

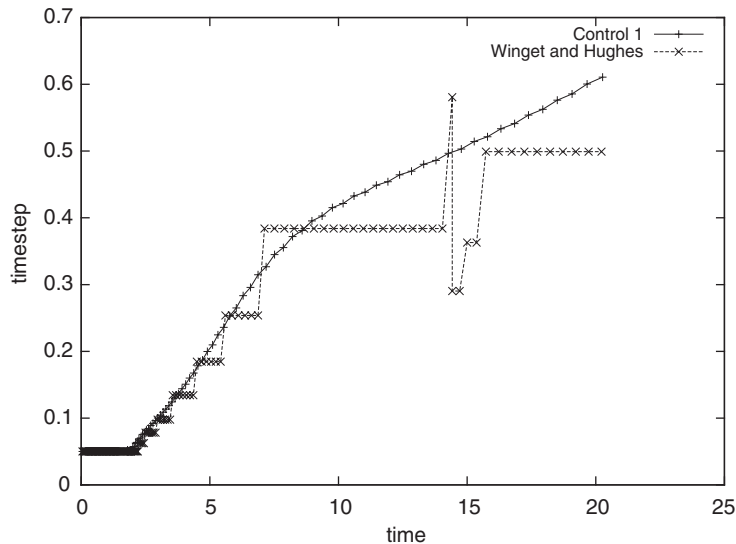


Figure 19. Timestep variation using Control 1 and W&H for the non-isothermal problem.

where $\partial\Omega_2$ is the right side of the dimensionless section $\Omega = [0, 1] \times [0, 1]$, $M_1 = \rho c_p L^2 / kt_s$, $M_2 = L^2 / \mathcal{D} t_s$, $Nu = h_g 2L / \mathcal{D}$ is the Nusselt number, $Sh = k_g 2L / \mathcal{D}$ is the Sherwood number, and $\phi = \sqrt{k_0 L^2 / \mathcal{D}}$ is the Thiele modulus. Here $k_0 = a \exp(-\gamma)$, $\gamma = \Delta E / \hat{R} T_0$ and $\beta = (-\Delta H_R) c_0 \mathcal{D} / k T_0$, where $-\Delta H_R$ is the heat of reaction.

We solve the unsteady problem with $M_1 = 176$, $M_2 = 199$, $Nu = 55.3$, $Sh = 66.5$, $\gamma = 20$, $\beta = 0.6$ and $\phi = 0.8$. The known steady-state velocity field is given by the numerical solution of a Stokes problem as in References [23, 24, 39] and input into the transport equations, which are solved for concentration and temperature. The approximate solutions are calculated using a grid with 8×8 bilinear elements. Figure 18 shows the transient temperature distribution in a catalyst section at times $t = 0, 1, 5$ and 10 .

For a fixed time equal to 20, we compare approximate solutions using Control 1 and W&H. We start with a timestep size of 0.05, and we allow minimum and maximum time steps of 0.05 and 5, respectively. The solutions are obtained with a tolerance of 10^{-6} for the changes in nodal temperature and concentration. Table VII shows the number of time iterations, ntstep, the number of rejected steps, nrejec, the number of Newton iterations, newt, and the computational effort, c_{effort} , defined as newt divided by the number of Newton iterations obtained using a fixed timestep size. We obtain the solution with 423 Newton iterations using

Control 1, and we need 1223 Newton iterations with a fixed timestep of 0.05. Thus, we have obtained this solution 2.89 times faster. W&H also produces good results. Figure 19 shows the timestep size against time for Control 1 and W&H. Observe that Control 1 produces a very smooth curve, while W&H yields a curve with several steps.

5. CONCLUSIONS

In this work we present two adaptive timestep selection schemes based on feedback control theory to increase the robustness of our finite element formulation of coupled incompressible viscous flow and transient heat and mass transfer with surface effects included. These PID control algorithms for timestep selection are based on controlling accuracy or the convergence rate of the successive iterations. The schemes were tested for Rayleigh–Benard–Marangoni flows, flow across a backward-facing step, unsteady flow around a circular cylinder and chemical reaction systems. The finite element flow formulation is based on a penalty Galerkin method and the transport equations utilize a SUPG formulation. The algorithm employs an iteratively decoupled scheme. In the application problems, we computed steady-state and transient solutions using fixed timestep sizes and adaptive timestep sizes to test the efficiency of our controllers to solve the related class of coupled problems. We also compared our controllers with a timestep selection algorithm from the literature.

One important issue is to assess solution accuracy when timestep control strategies are applied to a specified problem. In some of the examples, the controllers produced a smooth variation of timesteps. The results suggest that a robust control algorithm is possible. Further, computational cost of the selection procedures are negligible, since they involve only storing a few extra vectors, computation of norms and evaluation of kinetic energy. We demonstrate the efficiency of our first control to solve non-linear flow and reactive transport. In this example, efficient computation of the transport process demands the use of a timestep selection algorithm, since the process is highly non-linear because of an exponential chemical reaction term. The efficiency of Control 2 was verified in the numerical simulations of the Rayleigh–Benard–Marangoni problems, flow across a backward-facing step and unsteady flow around a cylinder. In all these problems Control 2 achieved the best performance. In some of the test problems, the choice of the timestep in Control 2 was dominated by the convergence rate of the successive iterations, and in other cases by the changes in the kinetic energy.

In closing we remark that the strategies here may be also applied in conjunction with adaptive mesh refinement. Here adaptive mesh refinement uses feedback control to monitor the error due to the spatial discretization and subdivides the mesh accordingly. One can then relate the error in the integration scheme specifically to the admitted error in the spatial discretization scheme to equidistribute the error in space and time. Another approach would be to use space–time finite elements in strips, with again the strip width (timestep) controlled using a PID approach. A more open question would be the application of PID ideas in an unstructured space–time formulation or in explicit–implicit hybrid integration schemes. The most recent development in the field of control theory for timestep selection is the use of digital filters [19]. They offer new possibilities which remain to be explored.

ACKNOWLEDGEMENTS

Dr Valli was supported by a CAPES grant from the Ministry of Education, Brazil, during her stay at the University of Texas at Austin. This work was developed under the Joint Cooperation Agreement between the University of Texas at Austin and COPPE, the Graduate School of Engineering of the Federal University of Rio de Janeiro, Brazil. This work has been supported in part by DoD High Performance Computing Modernization Program, US and CNPq/MCT, Brazil.

REFERENCES

1. Kahaner D, Moler C, Nash S. *Numerical Methods and Software*. Prentice-Hall, Inc.: Upper Saddle River, NJ, 1992.
2. Press WH, Teukolsky SA, Vetterling WT, Flannery BP. *Numerical Recipes in C—The Art of Scientific Computing* (2nd edn). Cambridge University Press: New York, NY, 1992.
3. Borse GJ. *Numerical Methods with Matlab—A Resource for Scientists and Engineers*. PWS Publishing Company: New York, NY, 1997.
4. Ralston A, Rabinowitz P. *A First Course in Numerical Analysis* (2nd edn). Dover Publications: New York, 2001.
5. Gresho PM, Sani RL, Engelman MS. *Incompressible Flow and the Finite Element Method—Advection–Diffusion and Isothermal Laminar Flow*. Wiley: Chichester, 1999.
6. Winget JM, Hughes TJR. Solution algorithms for nonlinear transient heat conduction analysis employing element-by-element iterative strategies. *Computer Methods in Applied Mechanics and Engineering* 1985; **52**:711–815.
7. Johan Z, Hughes TJR, Shakib F. A globally convergent matrix-free algorithm for implicit time-marching schemes arising in finite element analysis in fluids. *Computer Methods in Applied Mechanics and Engineering* 1991; **87**:281–304.
8. Jacob BP, Ebecken NFF. Adaptive time integration of nonlinear structural dynamic problems. *European Journal of Mechanics A—Solids* 1993; **12**(2):277–298.
9. Gustafsson K, Lundh M, Söderlind G. A PI stepsize control for the numerical solution for ordinary differential equations. *BIT* 1998; **28**:270–287.
10. Gustafsson K. Control theoretic techniques for stepsize selection in explicit Runge–Kutta methods. *ACM Transactions on Mathematical Software* 1991; **17**:533–554.
11. Gustafsson K. Control theoretic techniques for stepsize selection in implicit Runge–Kutta methods. *ACM Transactions on Mathematical Software* 1994; **20**:496–517.
12. Söderlind G. Automatic control and adaptive time-stepping. *Numerical Algorithms* 2002; **31**:281–310.
13. Valli AMP, Carey GF, Coutinho ALGA. Finite element simulation and control of nonlinear flow and reactive transport. *Proceedings of the 10th International Conference on Finite Element in Fluids*, Tucson, AZ, January 1998; 450–455.
14. Valli AMP, Carey GF, Coutinho ALGA. Control strategies for timestep selection in simulation of coupled viscous flow and heat transfer. *Communications in Numerical Methods in Engineering* 2002; **18**:131–139.
15. Valli AMP, Catabriga L, Coutinho ALGA. Acceleration strategies for solution of euler equations using an edge-based supg formulation with shock-capturing. *ECCOMAS Computational Fluid Dynamics 2001 Conference*, Swansea, Wales, UK, September 2001, CD-ROM.
16. Valli AMP, Coutinho ALGA, Carey GF. Adaptive control for time step selection in finite element simulation of coupled viscous flow and heat transfer. *European Conference on Computational Mechanics*, Munchen, Germany, August 1999, CD-ROM.
17. Valli AMP, Coutinho ALGA, Carey GF. Adaptive stepsize control strategies in finite element simulation of 2D Rayleigh–Benard–Marangoni flows. *15th Brazilian Congress on Mechanical Sciences*, Águas de Lindóia, SP, Brazil, November 1999, CD-ROM.
18. Valli AMP, Coutinho ALGA, Carey GF. Adaptive control strategies in finite element simulation of double diffusion and Marangoni convection problems. *Finite Elements in Flow Problems 2000*, Austin, TX, USA, April 2000; 71.
19. Söderlind G. Digital filters in adaptive time-stepping. *ACM Transactions on Mathematical Software* 2003; **29**:1–26.
20. Carey GF, Oden JT. *Finite Elements: Fluid Mechanics*, vol. 6. Prentice-Hall, Inc.: Englewood Cliffs, NJ, 1986.
21. Carey GF, Krishnan R. Penalty finite element methods for the Navier–Stokes equations. *Computer Methods in Applied Mechanics and Engineering* 1984; **42**:183–224.
22. Brooks AN, Hughes TJR. Streamline upwind/Petrov–Galerkin formulations for convection dominated flows with particular emphasis on the incompressible Navier–Stokes equations. *Computer Methods in Applied Mechanics and Engineering* 1982; **32**:199–259.

23. Irons BM. A frontal solution program for finite element analysis. *International Journal for Numerical Methods in Engineering* 1970; **2**:5–12.
24. Fellipa CA, Park K-C, Farhat C. Partitioned analysis of coupled systems. *Computer Methods in Applied Mechanics and Engineering* 2001; **190**:3247–3270.
25. Gustafsson K, Söderlind G. Control strategies for the iterative solution of nonlinear equations in ODE solvers. *SIAM Journal on Scientific Computing* 1997; **18**(1):23–40.
26. Powell JD, Franklin GF, Emami-Naeini A. *Feedback Control of Dynamic Systems*. Addison-Wesley Publishing Company: Reading, MA, 1994.
27. Coutinho ALGA, Alves JLD. Parallel finite element simulation of miscible displacements in porous media. *SPE Journal* 1996; **4**(1):487–500.
28. Bénard H. Les tourbillons cellulaires dans une nappe liquide. *Rev. Gén. Sci. Pure Appl.* 1900; **11**:1261–1271, 1309–1323.
29. Carpenter BM, Homsy GM. Combined buoyant-thermocapillary flow in a cavity. *Journal of Fluid Mechanics* 1989; **207**:121–132.
30. de Vahl Davis G. Laminar natural convection in a enclosed rectangular cavity. *International Journal of Heat and Mass Transfer* 1968; **11**:1675–1693.
31. Zebib A, Homsy GM, Meiburg E. High Marangoni number convection in a square cavity. *Physics of Fluids* 1985; **28**(12):3467–3476.
32. Griebel M, Dornseifer T, Neunhoffer T. *Numerical Simulation in Fluid Dynamics—A Practical Introduction*. SIAM: Philadelphia, PA, 1998.
33. McLay R, Carey GF. Coupled heat transfer and viscous flow, and magnetic effects in weld pool analysis. *International Journal for Numerical Methods in Fluids* 1989; **9**:713–730.
34. Armaly BF, Durst F, Pereira JCF, Schönung B. Experimental and theoretical investigation of backward-facing step flow. *Journal of Fluid Mechanics* 1983; **127**:473–496.
35. Gartling DK. A test problem for outflow boundary conditions—flow over a backward-facing step. *International Journal for Numerical Methods in Fluids* 1990; **11**:953–967.
36. Cruchaga MA. A study of the backward-facing step problem using a generalized streamline formulation. *Communications in Numerical Methods in Engineering* 1998; **14**:697–708.
37. Engelman MS, Jamnia M. Transient flow past a circular cylinder: a benchmark solution. *International Journal for Numerical Methods in Fluids* 1990; **11**:985–1000.
38. Dettmer W, Peric D. An analysis of the time integration algorithms for the finite element solutions of incompressible Navier–Stokes based on a stabilised formulation. *Computer Methods in Applied Mechanics and Engineering* 2003; **192**:1177–1226.
39. Petersen EE. *Chemical Reaction Analysis*. Prentice-Hall: Englewood Cliffs, NJ, 1965.
40. Finlayson BA. The method of weighted residuals and variational principles. *Mathematics in Science and Engineering*, vol. 87. Academic Press: New York, NY, 1972.
41. Bird RB, Stewart WE, Lightfoot EN. *Transport Phenomena*. Wiley: New York, NY, 1960.